EPJ Web of Conferences **74**, 01001 (2014)
DOI: 10.1051/epjconf/ 201474 01001

Measurement of G Using a Cryogenic Torsion Pendulum: Post-2008 Analysis Review

Riley Newman[1,a], Mike Bantel[2], Eric Berg[1], and Liam Cross[3]

[1] *Department of Physics and Astronomy, University of California Irvine, Irvine, CA 92697-4575, USA*
[2] *ExoAnalytic Solutions Inc., Mission Viejo, CA 92692, USA*
[3] *MongoDB, New York, NY 10036, USA*

Abstract. A measurement of G by our University of California, Irvine (UCI) team was reported at the 2008 Conference on Precision Electromagnetic Measurements (CPEM) [1]. This work has not yet been published; work continues to review and refine analysis of data from that measurement. We present in this paper the analysis and results of the measurement as it stood at the time of the 2008 conference, and discuss the analysis review under way. Our G measurement was conducted "blind", keeping the exact value of the source mass hidden until just before the conference presentation.

1 The Value of G

The world-wide effort to determine a more accurate value of G was inspired by the high precision measurement by Michaelis et. al. at the Physikalisch-Technische Bundesanstalt (PTB) in Germany in 1994 which reported $G = 6.71540(8.3)x10^{-11}\ \frac{m^3}{kg\ s^2}$ [2]. This was 6400 ppm larger than the earlier best measurement of $6.6726(50)x10^{-11}\ \frac{m^3}{kg\ s^2}$ by Luther and Towler at the National Institute of Standards and Technology (NIST) in the USA in 1982 [3]. Even today, the discrepancies among recent measurements persist.

The UCI measurement was unique among the handful of measurements conducted since then in that it used a cryogenic apparatus in an attempt to reduce thermal noise and systematic errors. Figure 1 displays recent measurements including the UCI triplet of values associated with data for three different torsion fibers reported at CPEM 2008.

2 The UCI Measurement

Torsion pendulum measurements use masses as a field source and pendulums as sensitive detectors, and extract the value of G through the static deflection angle, the force needed to maintain zero deflection, or shifts in pendulum oscillation frequency. The UCI measurement compared the oscillation frequency between two source mass positions. Details of the measurement and analysis formalism beyond what is presented here may be found in [5].

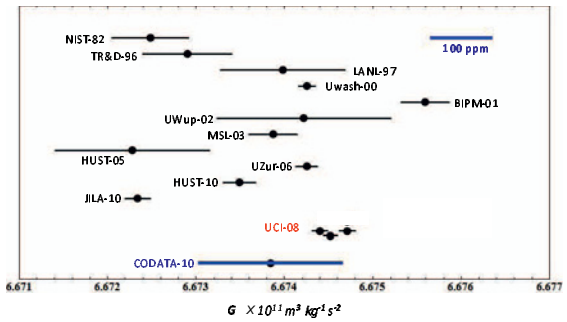

Figure 1. Recent Measurements of G, indicated by institution initials and year [4]. The UCI-08 points are results found with three different torsion fibers.

The source masses were two copper rings on opposite sides of the pendulum, far enough from the small pendulum that a multipole expansion of their interaction converges rapidly. The interaction is dominated by the coupling between the pendulum's quadrupole moment and the rings' gravitational field gradient. The rings had approximate mass 59 kg, outer diameter 520 mm, inner diameter 312 mm, thickness 48 mm, and were plated with non-magnetic NiP. Their spacing was such as to produce an extremely uniform field gradient near their midpoint - the first three spatial derivatives of the field gradient vanish at that point. Thus the measured frequency shift which results from the dominant coupling is very insensitive to pendulum positioning error (a 3 mm error in position results in less than a 1 ppm error in G).

The pendulum was chosen to be a thin plate because in the limit where the thickness goes to zero its torsional frequency shift when the source masses change position becomes independent of the shape and mass distribution

[a] e-mail: rdnewman@uci.edu

of the pendulum (See equation 1, in which q_{22} is the pendulum's quadrupole moment and I its moment of inertia). Several nearly identical pendulums were used in this work, made of fused silica with approximate dimensions 41 x 41 x 3 mm, and coated with aluminum or aluminum followed by gold.

$$\Delta\omega^2 \propto \frac{q_{22}}{I} = \frac{\int \rho(x^2 - y^2)dV}{\int \rho(x^2 + y^2)dV} \overset{y\to 0}{\longrightarrow} 1 \qquad (1)$$

The two source mass positions were 90 degrees apart as in figure 2. The difference in the pendulum's torsional frequency squared at the two positions is proportional to G. The ring spacing was maintained by two fused silica rods, 650 mm long and 8 mm diameter, contacting 5 mm diameter sapphire plates bonded to the rings.

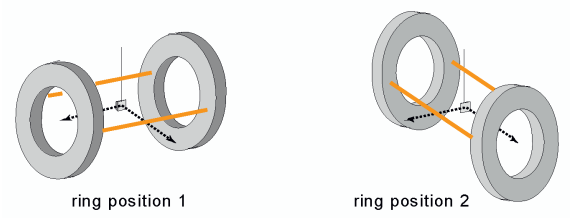

Figure 2. Diagram of source mass rings, positioning rods, and torsion pendulum in the two measurement positions 90 degrees apart.

Over 2000 hours of blind measurements were recorded during the four years: 2000, 2002, 2004, and 2006. The measured value of G was hidden from the team by using an approximate value for the total ring masses rather than the precisely measured value, and only revealed a few days before results were presented at the CPEM conference in 2008.

A number of variations were made throughout the experiment in order to check for systematic biases. These included: exciting the pendulum to one of five different amplitudes of torsional oscillation (0.3, 2.6, 4.2, 5.8, or 7.4 rad), suspending the pendulum from one of three different torsion fibers which provided the restoring force (CuBe as drawn, CuBe heat treated, or Al5056 as drawn), hanging one of three different pendulums or pendulum coatings (#1 with Al, #1 with Al and Au, or #2 with Al and Au), and orienting the rings by rotating them isomorphically into one of four different configurations (labelled $R1$, $R2$, $R3$ and $R4$).

The measurements were conducted in a remote location isolated from cultural noise, in a former Nike missile bunker in the desert of Washington State. The site was 6 km to the nearest public road and 20 km from the nearest city. The rainfall averaged only 20 cm/yr minimizing changes in the background gravitational gradient. The experimental site was on the lower slope of a basalt mountain, where microseismic ground motion was much lower than in the alluvial plain below it. The facility itself was about 5 m below ground level and surrounded by treeless grassland which minimized infrasonically coupled effects of variable winds. Figure 3 shows the location of this G lab from the top of the adjacent mountain relative to the LIGO gravitational interferometer (on an alluvial flood plane, with the Columbia River beyond that).

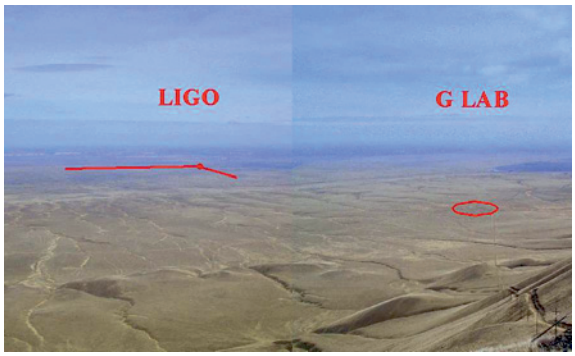

Figure 3. Photo of the desert wildlife preserve environment at the experimental site, indicated by the red circle.

The pendulum and fiber were maintained at fixed temperatures between 2.6 and 3.1 K. The rings and their positioning rods were located outside the cryogenic environment. Ring temperatures were monitored with platinum thermometers in small holes in the rings.

Torsion fiber properties change dramatically at low temperature. For example, quartz and tungsten fibers show low Q at low temperature despite being highly regarded for room temperature experiments, and sapphire shows a nonlinear dependence of Q^{-1} on oscillation amplitude. The choice of copper-beryllium and aluminum fibers in this measurement was based on preliminary studies showing high tensile strength and high Q. Our torsion pendulums using these fibers have a very large Q factor (~100,000), which together with the low temperature greatly reduces the thermal noise contribution (see equation 2). These materials are also electrically conductive, allowing any static charges to bleed off the pendulum, minimizing electrostatic forces. Additional advantages of a cryogenic environment are that the thermal control can be maintained very precisely (~5 uK over 24 hrs) and the torsion constant of a fiber is less sensitive to temperature variation. Practically speaking it also provides an excellent vacuum (well below 10^{-6} mBar) through cryopumping action as well as excellent magnetic shielding with lead foil which is superconducting at 7.2 K.

$$\tau_{noise} \propto \sqrt{\frac{k_B T}{Q}} \qquad (2)$$

The cryostat consisted of a large stainless steel vacuum canister at the end of long thin-wall pumping tubes immersed in liquid helium in a ~3 m tall dewar. Additional cooling was obtained with a commonly used technique by pumping on a continuous-fill liquid helium reservoir within the vacuum canister. Temperature stability was achieved with proportional-integral-differential (PID) feedback control on the pumping impedance as well as PID control of two independent staged heaters leading to

the fiber support. In vacuum at this temperature, the pendulum's thermal fluctuations are dominated by conduction down the fiber. Figure 4 shows the cryostat assembly along with the following auxiliary systems. The vacuum was established with an ion pump but maintained through passive cryopumping throughout much of the G datataking. The cryostat angular positioning was set with a rotation bearing and its tilt was monitored with cryogenic tiltmeters. In order to reduce swinging of the pendulum, a magnetic eddy current damping disk inside a return yolk joined a stiff upper fiber to the thin lower torsion fiber. The pendulum motion was measured using an infrared optical lever, conveyed into the cryogenic environment by fiberoptic and detected there with a split photodiode after reflecting off one or more mirrors. The source mass rings were positioned with a separate rotating turntable from which they hung by Kevlar strings. These components are detailed in figure 4.

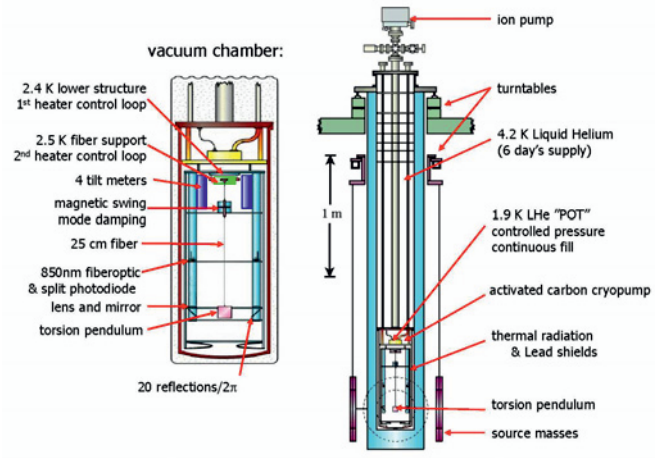

Figure 4. Diagram of cryostat and auxiliary components.

The apparatus, pictured in figure 5, was decommissioned and recycled in September 2011 after being used to conduct an inverse-square-law-violation test with Paul Boynton of the University of Washington (also reported on in these proceedings) [6].

Figure 5. Photos of the cryostat in situ, as seen from the underground laboratory's main floor and from a subfloor below.

3 Analysis up to 2008

The fundamental measurement involved here is a timing measurement. The pendulum's angular position in time is determined through a set of 20 reflections per revolution registered by the optical lever, and from these the period and thus frequency shift is calculated. G is then determined from the frequency shift along with the ring field moments and pendulum multipole moments calculated from knowledge of their mass distributions and relative positioning. The magnitudes involved in this timing measurement are illustrated by the example data in figure 6 from run #16. Data was acquired in independent runs lasting about two days. The pendulum amplitude was re-excited to a nominal value between runs. The source mass rings were moved between the two positions every 12 to 24 torsional periods (more for early runs such as #16). The pendulum torsional period was between 105 and 135 sec depending on the support fiber. The change in the pendulum's torsional period when the rings were moved between the two positions shown in figure 2 was between 0.2 and 1.7 msec depending on torsional amplitude and fiber. This very small period shift is the price paid for the large separation between source mass and pendulum, imposed by the size of the cryogenic dewar. For a torsional period of 113 sec and signal period shift as small as 0.2 msec, to measure G to 5 ppm the period shift must be measured to 5 ppm. Thus the reference clock frequency needs to be accurate to just a few ppm but stable over periods of an hour to better than one part in 10^{11}. These requirements were satisfied by our HP58503B GPS-steered crystal oscillator reference clock.

The apparatus was sealed up and cooled to low temperature prior to data-taking on six occasions over the 2000-2006 time period. As described in Sect. 2, changes in fiber, pendulum and temperature setpoint characterize each cooldown period. Table 1 presents this information along with related characteristics and gives a global view of the UCI G measurement effort.

A thorough understanding of the pendulum's motion is required in order to extract the signal coupling while excluding other perturbations. The general equation of motion for the torque in equation 3 contains terms accounting for the nonlinearity of the fiber's restoring torque (k_1, k_2, k_3), anharmonic behavior (k_{ss}), damping (b) due to internal friction in the fiber, and any torque periodic in rotation angle such as the gravitational coupling to the source mass rings or to external background fields.

$$I\ddot{\theta} = -[k_1\theta + k_2\theta^2 + k_3\theta^3 + b\dot{\theta} + k_{ss} f_D(\theta,\dot{\theta}) + \sum_m \alpha_m Cos\,(m\theta) + \sum_m \beta_m Sin\,(m\theta)] + ... \quad (3)$$

The first-order solution to equation 3 is given by equation 4 where A is the torsional amplitude. High precision numerical integrations of equation 3 demonstrate that this first order solution is adequate for our purposes.

Table 1. Summary of cryogenic data sets. Aluminum fibers were preferred above the others due to the high Q and low amplitude dependance of Q^{-1}, suggesting smaller (unknown) systematic fiber effects. The three datasets leading to reported G values are numbered beside the dates. Not represented in this table are about 415 hours of data were collected in 2004, using the #1 pendulum after it was damaged in the process of adding gold plating and later repaired. This data suffered from extreme noise believed to be due to a leak in the dewar's evacuated insulating wall gap. The dewar was replaced before the 2006 runs.

	dates	pendulum	fiber	period, Q and temperature	ring configuration	# runs
#1	9 to 11/2000	#1 with Al	20 μm CuBe as drawn	135 sec, 80k, 2.6 K	R1,R2,R3,R4	23
#2	12/2000	#1 with Al	20 μm CuBe heat treated	130 sec, 120k, 2.7 K	R1,R2	9
#2	3 to 5/2002	#1 with Al	20 μm CuBe heat treated	130 sec, 120k, 3.1 K	R1,R2,R3,R4	39
#3	3 to 5/2006	#2 with Al+Au	25 μm Al5056 #2	113 sec, 170k, 2.9 K	R1	36

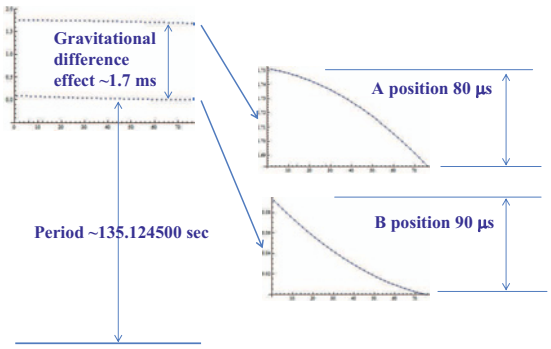

Figure 6. Torsional period variation with time for run #16, as the torsional amplitude decays from 2.69 to 2.54 rad over 74 hrs. The expanded scale to upper left shows the 1.7 msec shift in period as the rings assume alternate positions. The further greatly expanded scales to the right show the period variation due to a combination of secular period drift associated with fiber relaxation and the variation with decaying amplitude in the Bessel function dependence seen in equation 4 (note the opposite curvature in the two subplots). The secular drift is nearly linear, and is largely removed in our analysis by an "aba" treatment in which the torsional period P_1 measured at one of the ring pair's positions is compared to the average of the periods measured with the other ring position just before and just after P_1 was measured. The Bessel function amplitude dependence is treated explicitly in our analysis in terms of measured amplitudes.

$$\omega^2 \approx \omega_0^2\left[1 + \frac{3}{4}A^2\frac{k_3}{k_1} - 2A\frac{k_{ss}}{k_1} + \frac{2}{A}\sum_m J_1(mA)\frac{\beta_m}{k_1}\right] \quad (4)$$

Taking the difference between this frequency squared at the two source mass ring positions gives the signal term in equation 5 neglecting the various systematic perturbations. Here S is determined from measured timing differences and K is the expected value of S if $G = 1$, as calculated from metrology and positioning in terms of the pendulum quadrupole moment q_{22} and source mass field moment a_{22}. Due to the ring shape, ring positioning, and pendulum symmetry, higher order multipole terms ($m > 2$) contribute about 6 ppm to the calculation of G, dominated by the β_6 term; the others totaling no more than 1 ppm.

$$\begin{aligned}
\Delta\omega^2 &= \frac{4\beta_2}{I}\frac{J_1(2A)}{A} \\
S &= \frac{\Delta\omega^2 A}{2J_1(2A)} \approx \frac{2\beta_2}{I} \\
K &\approx \frac{2\beta_2}{I}(calculated\ with\ G = 1) \\
G(measured) &= S/K
\end{aligned} \quad (5)$$

In addition to the torque terms made explicit in equation 3 there is a dissipative mechanism which Kuroda [7] has pointed out leads to a G measurement bias which, with a reasonable choice of parameters, implies that a measured G will be too large by $\frac{\delta G}{G} = \frac{1}{\pi Q}$, where P is the period. We have shown that in the framework of the widely used model for dissipation discussed by Kuroda the effect on G must be bounded by $0 \le \frac{\delta G}{G} \le \frac{1}{2Q}$ [8]. Obtaining a high Q to minimize this G bias was our main motive for working at low temperature. For the dissipative term f_D in equation 3 we assume a frequency-independent stick slip mechanism for which we have strong evidence. The mechanism predicts a linear dependence of Q^{-1} on oscillation amplitude, and a certain ratio between $\frac{dQ^{-1}}{dA}$ and $\frac{dQ^{-1}}{d\omega^2}$, both observed in our previous study of fiber properties [9]. The linear variation of dQ^{-1} in our G data is displayed in figure 7.

To check for systematic biases that might be revealed through different effects when operating at different torsional amplitudes, data was collected at a variety of oscillation amplitudes, selected for their large signal and high signal/noise ratio as indicated in figure 8. All but the lowest of these amplitudes are near extrema of the frequency shift, making the G measurement less sensitive to amplitude determination inaccuracy.

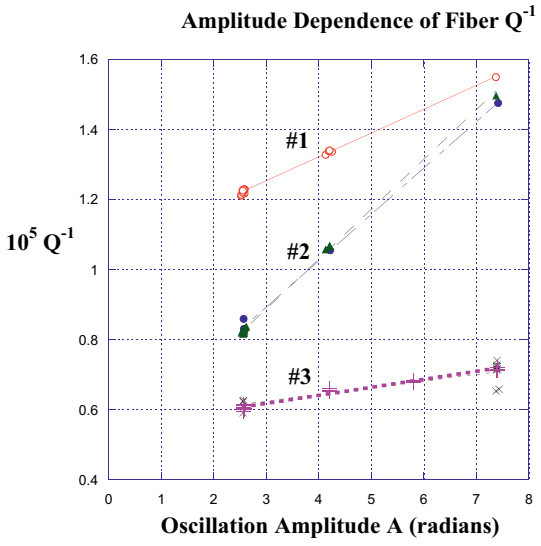

Figure 7. Fiber $Q^{-1}(A)$ linear dependence for the three G dataset fibers: #1 CuBe as drawn, #2 CuBe heat treated, and #3 Al5056. The two datasets in #2 correspond to data taken in years 2000 and 2002.

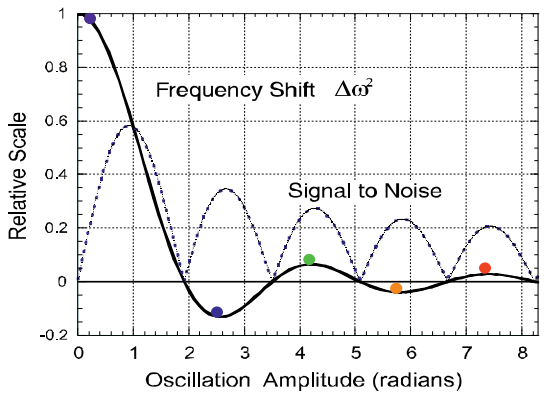

Figure 8. Frequency shift size and signal/noise as a function of amplitude, showing the five values where G data was acquired. The relative signal size is simply proportional to the function $J_1(2A)/A$

The blind results of the measurement of S relative to a hidden S_{ref} for the amplitudes and fibers used in the three G datasets are shown in figure 9. The values as acquired in time for individual runs are shown in figure 10, color-coded for amplitude. The mean values for three fiber types are shown as horizontal black lines. These values are histogrammed in figure 11. Note the uncertainties in these plots are purely statistical and that the metrology leading to the value of K is not yet involved. The noise seen in these measurements exceeded the value expected from thermal kT noise by more than an order of magnitude. Although the dominant source of the statistical noise was never identified after many years of tests, it seems that the only possible significant external sources are the mHz vibrations of the instrument caused by extremely low frequency microseismic background and infrasonic coupling to wind.

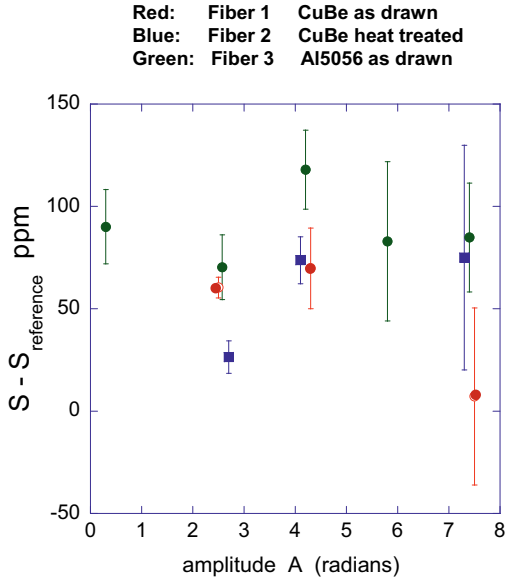

Figure 9. Signal S relative to a hidden constant S_{ref} as a function of amplitude, averaged over runs for a given fiber and amplitude as presented at CPEM 2008.

Details of the uncertainty budget resulting from the metrology and all other significant sources are summarized in tables 2, 3 and 4. Background gradient changes due to rainfall were negligible. Electrostatic fields were found to be negligible by varying the potential of the pendulum's immediate environment, a gold plated copper cylindrical shield.

Table 2. The source mass ring contribution and uncertainty budget, as presented at CPEM 2008.

ppm	correction	error (ppm)
ring mass	—	3.9
ring dimensions	—	2.8
string slot	140.1	1.8
kevlar string	19.0	0.1
outer chamfers	36.2	0.9
inner chamfers	-28.7	0.8
sapphire contact plates	27.9	2.2
Pt thermometers	3.5	0.2
swing monitor mirror	1.0	0.0
NiP plating	0.5	0.3
rod end shapes	-12.1	1.0
ring radial taper	24.2	1.0
rod radial position	—	1.2
rod length	—	3.6
suspension misalignment	10.7	4.0
SUBTOTAL	~220	~8.0

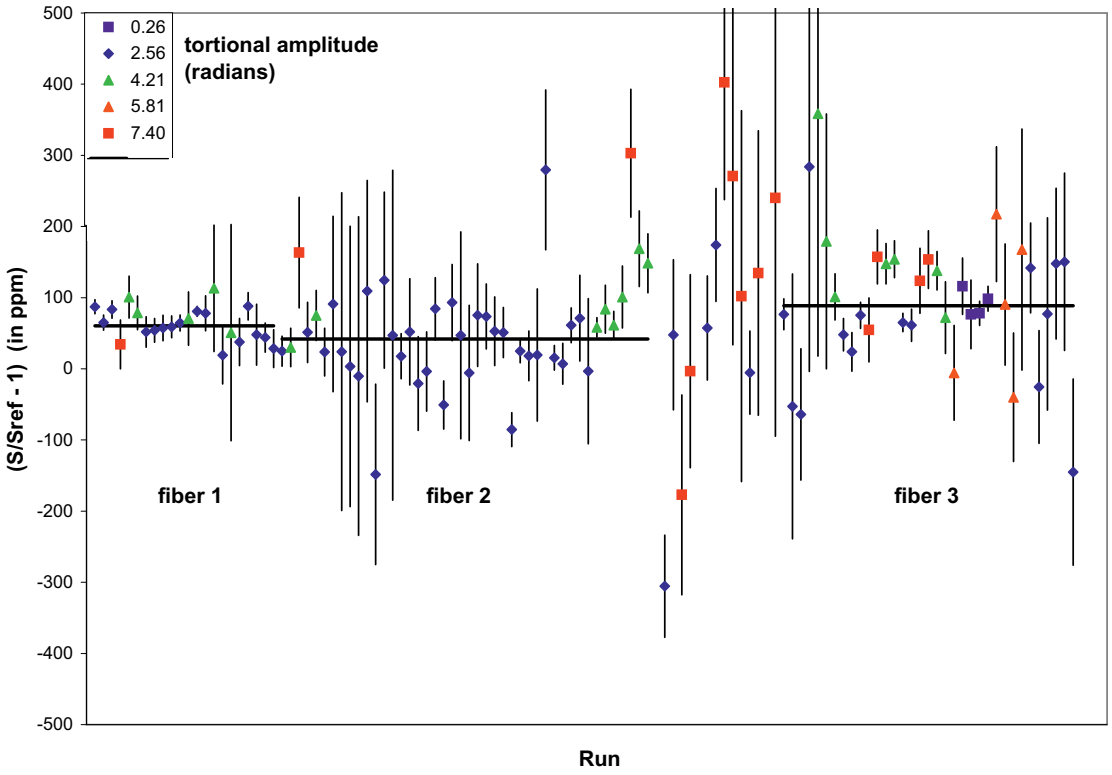

Figure 10. Signal S relative to a hidden constant S_{ref} in time between 2000 and 2006 for sequential runs as presented at CPEM 2008. Three extreme outlier points are not shown.

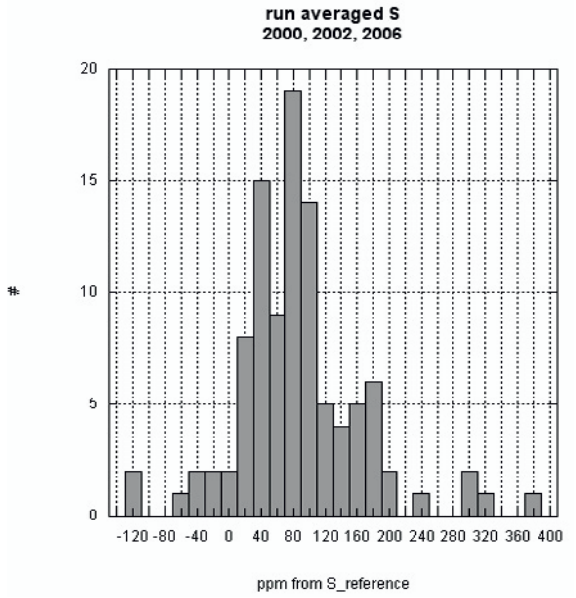

Figure 11. Histogram of signal values S relative to a hidden constant S_{ref} as presented at CPEM 2008.

Table 3. The pendulum contributions and uncertainties, as presented at CPEM 2008.

corrections	fiber 1	fiber 2	fiber 3	ppm
width	0	0	13.1	±0.4
thickness	0	0	-91.5	±2.7
chamfers	30.0	30.0	33.5	±0.6
coatings	-1.4	-27.3	-26.9	±0.7
fiber attachment (screw, ferrule, glue)	-14.7	-19.8	-17.7	±2.1
chip repair		-1.9		±1.0
SUBTOTAL	13.9	-19.0	-89.5	±3.7

Table 4. Spurious torque contribution and uncertainty budget for other systematics. The lower rows apply to all fibers, as presented in 2008.

corrections	fiber 1	fiber 2	fiber 3
k_3	-0.2±0.2	-1.0±0.5	-0.5±0.2
k_{ss}	-0.5±0.5	-2.4±2.4	-0.5±0.5
anelasticity $1/(\pi Q) \pm 1/(4Q)$	4.3±3.3	3.4±2.7	2.1±1.7
ambient gravity	0.0±1.0	0.0±1.0	0.0±1.5
magnetic coupling	2.0±1.0	-2.0±1.0	0.0±0.5
SUBTOTAL	5.6±3.6	-2.0±3.9	1.1±2.4
pendulum tilt	±0.1-5.4		
X,Y,Z,ϕ alignment	±0.1-3.6		
turntable accuracy	±1.0		
air density	±1.3		
ring temperature	±1.5		
ring configurations	±7.5		
SUBTOTAL	±7.8-10.1		

Once the value of K is determined and combined with S, three values of G emerge with individual uncertainties lower than previous measurements of G. However the three values disagree significantly. The three values reported in 2008 are displayed in figure 12. Faced with this likely systematic bias and with no clear understanding of its source other than the fibers themselves, we combined the three into a value centered on the third set's result with assymetric uncertainty as shown in table 5. We chose this in the days before CPEM 2008 because we considered that dataset to be the least susceptible to systematic error arising from fiber properties: the Al50506 fiber exhibited a smaller $Q^{-1}(A)$ dependance and a higher Q value.

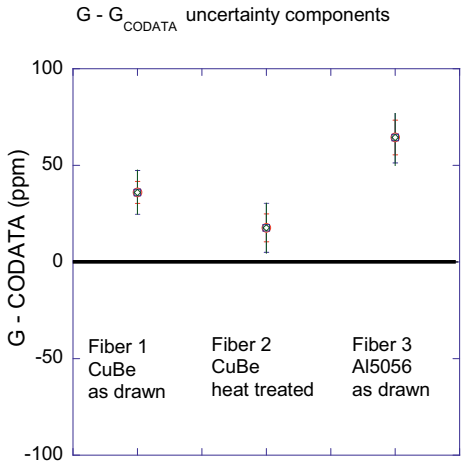

Figure 12. UCI G results presented in 2008 relative to the 2006 CODATA value for the three fibers.

Table 5. The three UCI G results as reported at the CPEM 2008 conference, but here relative to the 2010 CODATA value. Analysis of our work continues, and these values will change somewhat.

uncertainties	fiber 1	fiber 2	fiber 3
torques	±3.6	±3.9	±2.4
metrology	±9.2	±9.7	±9.2
statistical	±5.7	±7.2	±9.0
SUBTOTAL	±11.4	±12.7	±13.1
fiber-type			+20-40
TOTAL			+25-42
G - CODATA	+102 ppm	+84 ppm	+130 ppm
$Gx10^{11}\ \frac{m^3}{kgs^2}$	6.67452(8)	6.67440(8)	6.67471(9)

4 Analysis Review Since 2008

The preceeding section describes our analysis and results presented at the CPEM 2008 conference. In our rush to prepare results, we identified specific checks that needed to be more carefully examined to be sure no mistakes were made. Here we report on an ongoing effort to review that analysis. The review so far has resulted in four areas of concern which only slightly alter the results announced in 2008, as described in the following sections.

4.1 Calculation Code Mistakes

A pair of code errors identified after the 2008 presentation were found that will shift our G values by about 3 ppm.

As we continue to refine our data analysis we add a different pseudo-random number to the G values found with the different fibers to largely hide the effect of varying our analysis procedures as described in the following section. We expect to reveal our final G values found with the three fibers in 2014 at a conference specifically addressing measurement of G.

4.2 Averaging Over Source Mass Configurations

Figure 13 illustrates the rotations which move the rings isomorphically from one configuration to another of the four used in data-taking ($R1$, $R2$, $R3$, $R4$). The form of our rings was measured for us by NIST. The rings have fabrication imperfections such that their thickness varies with R and θ by as much as 20 μm, which if not taken into account would produce G error on the order of 50 ppm. By making unweighted averages of G found with the four configurations we arrive at a value that needs correction only for average variation of ring width with radius, which we know very precisely from the NIST data supplemented by measurements made at UCI. We are reviewing this procedure, which is limited by unequal numbers of good data in the four configurations, and are considering replacing that approach with one in which fits of NIST data are used in finding G separately for each ring configuration.

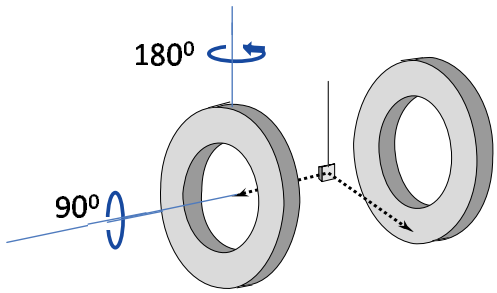

Figure 13. The source mass rings were individually rotated about two axes in order to form a set of four unique ring configurations: *R*1, *R*2, *R*3 and *R*4.

4.3 Rejection of Background Frequency Drift

Our analysis used an "aba" approach to eliminate the effect of *linear* background frequency variation in time, but this does not cancel higher order background variation. Perhaps we need an "abab" or higher order scheme? Or a background subtraction based on the average of separate fits to each ring position dataset. Figure 14 illustrates the "aba" averaging used to determine the period shift, and figure 15 illustrates the background fit subtraction approach. When this approach is applied to run #16 the result is shown in figure 16 (compare this with figure 6).

This has a slight effect on two of our fiber dataset results.

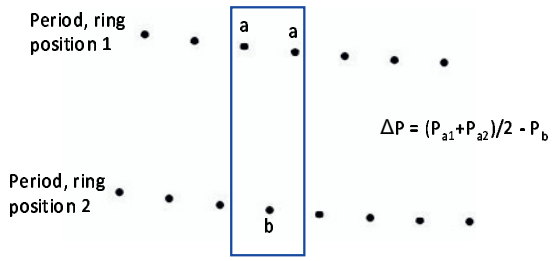

Figure 14. Illustration of the "aba" method to remove linear background drifts.

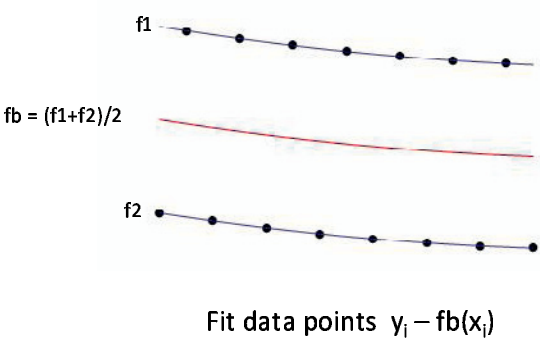

Figure 15. Illustration of the background fitting method.

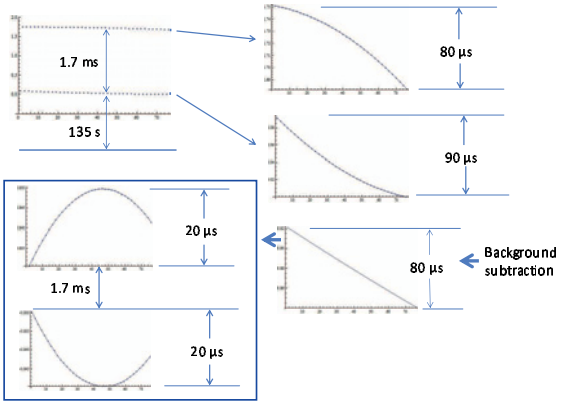

Figure 16. Run 16 data showing the effect of the background fitting method.

4.4 Accuracy of Amplitude Determinations

Did we measure torsional amplitude accurately enough? Refer back to figure 8 to see how misjudging the amplitude can directly affect the expected period shift and thus the inferred value of *G*. Amplitudes are calculated using the 20 reflections per revolution caused by 8 auxiliary mirrors. Figure 17 illustrates how this optical lever scheme works and figure 18 shows how these reflections are fit to get the torsional amplitudes. Equation 6 indicates the reference used for calibration of different amplitude datasets.

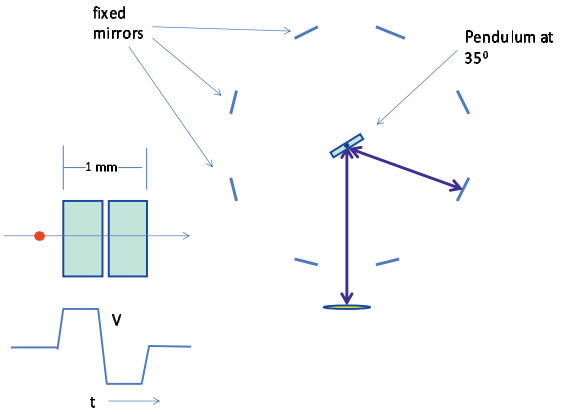

Figure 17. Optical lever mirror construction resulting in 20 reflections hitting the split photodiode.

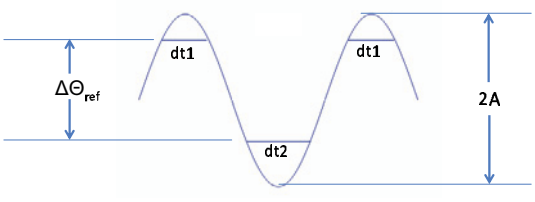

Figure 18. Illustration of how oscillation amplitudes are fit from multiple reflections recorded by the optical lever data aquisition.

$$A = f\left(dt1, dt2, \Delta\Theta_{ref}\right)$$
$$if\ A > \pi, \Delta\Theta_{ref} = 2\pi$$
$$if\ A > 2\pi, \Delta\Theta_{ref} = 2\pi\ or\ 4\pi$$
$$if\ A < \pi,\ need\ to\ calibrate\ \Delta\Theta_{ref}\ relative\ to\ 2\pi \quad (6)$$

What about harmonics? Recall equation 3. The solution for $\theta(t)$ includes several harmonics due to fiber nonlinearity as well as due to the G signal itself. These are tabulated in table 6.

Table 6. Harmonics of concern in the pendulum motion.

amplitude	source	c_2 (μrad)	c_3 (μrad)	c_5 (μrad)
2.6 rad	k_2	-0.4		
	k_3		-0.02	
	β_2		+3.9	+1.1
7.4 rad	k_2	-2.9		
	k_3		-0.5	
	β_2		-2.5	+0.6

$$\theta = AS\,in\,(\omega t) + c_2 Cos\,(2\omega t) + c_3 S\,in\,(3\omega t) + c_5 S\,in\,(5\omega t)$$

Because of concerns that harmonics are dangerously affecting our amplitude measurements, we have experimented with letting amplitude be a free parameter in fitting data to extract G. However, we have found with simulations including harmonics that we are calibrating the reference angle used to calculate amplitudes less than π to better than 1 μrad. The effect of harmonics in using that reference angle to determine amplitudes in our G data produces a greater error, of about 4 μrad in measured amplitude values. This contributes an uncertainty of less than 1 ppm in our measurement of G.

5 Summary

Measurement of G is notoriously difficult and reanalysis or review of analysis years after first reported results are not unusual. The UCI measurement of G with a cryogenic torsion pendulum was first reported in 2008 to be $6.67471 + 0.00017 - 0.00028\ x10^{-11}\ \frac{m^3}{kg\,s^2}$. Since then we have reviewed a number of areas of our analysis and identified four areas of concern, and have extended our formerly blind analysis in an essentially blind fashion. At this time we expect changes in G values found with each fiber type to have magnitude less than about 15 ppm and individual changes to our uncertainties to have magnitude less than about 10 ppm. We anticipate presenting the concluding analysis review and final G result at a conference February 27th 2014 dedicated to measurement of G.

6 Acknowledgments

We thank Roy Gephart and the Pacific Northwest National Lab for hosting the experimental site; Paul Dunn, Haskell Sheinberg and Bill Baker and the Los Alamos National Lab for the source mass fabrication; Zeina Jabbour, Howard Harary, and Dennis Everett and the NIST for ring mass and dimensional measurement; the many researchers, students and staff at UCI over the past 18 years; and Karim Munawar, Yao Cheng and Ignazio Ciufolini for arranging the International Symposium on Experimental Gravitation and these proceedings. This research was conducted with funding from the National Science Foundation (including grant #0404514).

References

[1] M.K.Bantel et. al., "25th Conference on Precision Electromagnetic Measurements." 8-13 June 2008. Broomfield, Colorado, USA. (http://www.icpem.org/2008/), (2008).

[2] W. Michaelis et. al.,"18th Conference on Precision Electromagnetic Measurements." 27 June - 1 July 1994. Boulder, Colorado, USA. (1994).

[3] G. Luther and W. Towler, Phys. Rev. Lett. **48**, 121-123 (1982)

[4] CODATA-10 = P.J. Mohr et.al., Rev. Mod. Phys. **84**, 1527-1605 (2012)

[5] R. Newman et. al., Meas. Sci. Technol., **10**, 445-453 (1999)

[6] R. Newman et. al., Space Sci. Rev. **148**, 175-190 (2009)

[7] K. Kuroda, Meas. Sci. Tech. **10**, 435-438 (1999)

[8] R.D. Newman and M.K. Bantel, Meas.Sci.Technol. **10**, 445-454 (1999)

[9] M.K. Bantel and R.D. Newman, J. Alloys and Comp. **310**, 233-242 (2000)